Origin of magnetic mineral concentration variation in the Southern Ocean

Toshitsugu Yamazaki[1] and Minoru Ikehara[2]

Received 21 December 2011; revised 10 March 2012; accepted 13 March 2012; published 24 April 2012.

[1] In the Southern Ocean, magnetic mineral concentration increases in glacial periods. The variation pattern closely resembles eolian dust flux records from Antarctic ice cores, but the cause of the linkage remains unclear, as the dust flux is too small for the source of terrigenous materials in the Southern Ocean. We have conducted an environmental magnetic study of late Pleistocene sediments from the south Indian Ocean to investigate the origin of the magnetic concentration changes. Biogenic magnetites can be detected using the characteristics of almost no magnetostatic interactions and narrow coercivity distribution, reflecting occurrence of single-domain magnetites in a chain. We interpret that a non-interacting component on first-order reversal curve diagrams and low-coercivity components with small dispersion from isothermal remanent magnetization (IRM) component analyses represent biogenic magnetites, and that the interacting and middle-coercivity components represent terrigenous maghemites. The ratio of anhysteretic remanent magnetization susceptibility to saturation IRM reflects relative abundance of the biogenic and terrigenous components. It was revealed that biogenic magnetites are a dominant constituent of the magnetic minerals. In glacials, the abundance of both biogenic and terrigenous components increased with increased proportions of the latter. Increased ocean productivity in glacials is suggested from increased proportions of biogenic magnetites with elongated morphologies, indicative of less-oxic conditions, and increased sedimentation rates. These observations suggest that the increased magnetic concentration in glacials in the Southern Ocean may be explained by iron fertilization; the production of biogenic magnetites was enhanced associated with increased ocean productivity, which was fueled by increased eolian dust flux.

Citation: Yamazaki, T., and M. Ikehara (2012), Origin of magnetic mineral concentration variation in the Southern Ocean, *Paleoceanography*, *27*, PA2206, doi:10.1029/2011PA002271.

1. Introduction

[2] The Southern Ocean plays a key role in the Earth's climatic system, and has become a focus of paleoceanographic research. Oceanography of this province shows zonal characters circling Antarctica; the Subtropical Convergence and Polar Front occur along ~40°S and ~50°S latitudes, respectively (Figure 1). The Antarctic Circumpolar Current (ACC) flows eastward approximately between 45°S and 55°S, driven mainly by westerly winds that circle Antarctica [*Carter et al.*, 2008]. The ACC distributes substantial part of the North Atlantic Deep Water (NADW) from the Atlantic to other oceans.

[3] In the Southern Ocean as well as in the Atlantic, it is known that magnetic mineral concentration, represented by rock-magnetic parameters such as magnetic susceptibility and isothermal remanent magnetization (IRM), increases in glacial periods [e.g., *Kent*, 1982; *Robinson*, 1986; *Dezileau et al.*, 2000; *Diekmann et al.*, 2000; *Schmieder et al.*, 2000]. Conspicuous coincidence of the variation patterns between eolian dust flux in the Vostok and EPICA Dome C (EDC) ice cores and magnetic susceptibility of sediment cores in the Southern Ocean including the south Indian Ocean, southwest Pacific, and Scotia Sea near the Antarctic Peninsula has been noticed repeatedly [*Petit et al.*, 1990; *Bareille et al.*, 1994; *Pugh et al.*, 2009; *Weber et al.*, 2012]. The similarity ranges not only glacial-interglacial variability, but also shorter timescale fluctuations during glacial periods. The susceptibility-dust linkage is utilized for inter-core correlation of the circum-Antarctic scale and age estimation, which is otherwise difficult because generally poor preservation of calcareous microfossils in sediments south of the Polar Front prevents oxygen isotope stratigraphy. The cause of the linkage is, however, not straightforward and remains unclear at present. The eolian dust flux observed in the ice cores is far less than sufficient for being a dominant source of terrigenous flux in the marine sediment cores [*Bareille et al.*, 1994; *Pugh et al.*, 2009], and hence it was concluded that eolian dust is not important as a source of magnetic minerals.

[1]Geological Survey of Japan, National Institute of Advanced Industrial Science and Technology, Tsukuba, Japan.
[2]Center for Advanced Marine Core Research, Kochi University, Kochi, Japan.

0883-8305/12/2011PA002271

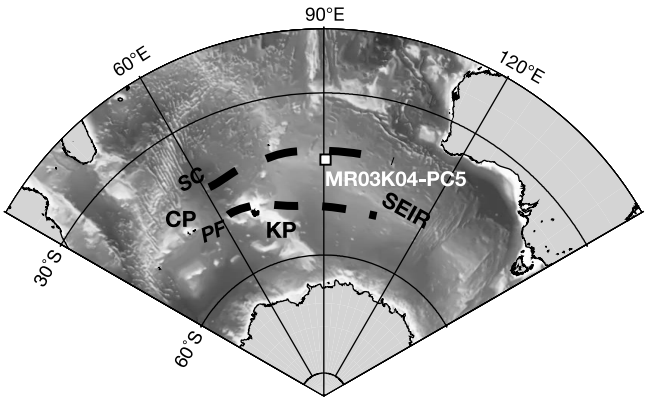

Figure 1. Location of core MR03K04-PC5. SC: Subtropical Convergence, PF: Polar Front (simplified after *Orsi et al.* [1995]), SEIR: Southeast Indian Ridge, KP: Kerguelen Plateau, CP: Crozet Plateau.

[4] Rock-magnetic techniques are increasingly utilized for paleoclimatic and paleoceanographic studies [e.g., *Verosub and Roberts*, 1995; *Evans and Heller*, 2003; *Watkins et al.*, 2007; *Suganuma et al.*, 2009], although applications to sediments in the Southern Ocean is still underrepresented [*Mazaud et al.*, 2007, 2010; *Venuti et al.*, 2011]. Recent development of environmental magnetism has made it possible to evaluate contribution of biogenic magnetites in magnetic mineral assemblages of sediments [*Egli*, 2004a, 2004b; *Yamazaki*, 2008, 2009; *Egli et al.*, 2010; *Roberts et al.*, 2011; *Yamazaki*, 2012]; this makes use of the characteristics of biogenic magnetites, that is, narrow coercivity distribution and very small magnetostatic interaction, which comes from the occurrence of biogenic magnetites within a narrow single-domain (SD) size range as chains. These characteristics can be detected from first order reversal curve (FORC) diagrams, component analyses of remanent magnetization acquisition/demagnetization, and the ratio of anhysteretic remanent magnetization (ARM) susceptibility to saturation IRM (k_{ARM}/SIRM).

[5] We have conducted an environmental magnetic study of a sediment core taken from the south Indian Ocean. We present that the magnetic mineral assemblage in the core are dominated by biogenic magnetites, and propose a possibility that productivity of magnetotactic bacteria driven by iron fertilization mainly controls magnetic mineral concentration variations in the Southern Ocean.

2. Material and Age Control

[6] Core MR03K04-PC5 (~6.7 m in length) was obtained from the northern flank of the Southeast Indian Ridge at 41°33.07′S, 90°24.39′E (Figure 1) using a piston corer during the cruise MR03-K04 Leg 6 of R/V *Mirai* in 2004. The site is within the subantarctic zone between the Subtropical Convergence and Polar Front [*Orsi et al.*, 1995]. The water depth of the coring site is 2913 m, which is above the present carbonate compensation depth (CCD) there. The core is dominated by foraminifer-bearing nannofossil ooze. Foraminifera and nannofossils are abundant and well preserved throughout the core. The core was physically disturbed moderately during coring near the top of the core and between about 4.0 and 4.5 m in depth; the latter was due to deformed core liner. The occurrence of the Fe-redox boundary at a depth of 4.3 m is recognized visually as a brown-to-gray sediment color change, which is documented clearly in color reflectance variations measured onboard at 2 cm intervals on split core surfaces through transparent polyethylene wrap using a photospectrometer (Minolta CM-2002) (Figure 2a). The location of the Fe-redox boundary is supported also by low-temperature magnetic properties, which is presented later.

[7] Discrete samples for rock-magnetic and isotopic measurements were taken onboard from the split core surface using plastic cubes (7 cm^3). The samples were collected continuously with gaps between samples being minimized. The samples were tightly sealed to prevent dehydration and were kept refrigerated.

[8] Oxygen-isotope ratios ($\delta^{18}O$) were measured on planktonic foraminifera *Globigerina* (250–355 μm in test size) at about 4.6 cm intervals except for the top 1 m of the core, where the measurements were carried out at about 2.3 cm intervals, using a mass spectrometer IsoPrime. The $\delta^{18}O$ variations can be correlated to the standard SPECMAP stack [*Imbrie et al.*, 1984] (Figure 3). The bottom of the core reached to the Marine Isotope Stage (MIS) 12, approximately 450 ka. The average sedimentation rate throughout the core is 15.1 m/Myr. The sedimentation rates during glacial periods are somewhat relatively higher than interglacials in general (Figure 3). The sedimentation rate appears to increase upcore, but this might have been caused by oversampling of a piston corer [*Skinner and McCave*, 2003; *Széréméta et al.*, 2004; *Yamazaki and Kanamatsu*, 2007].

3. Methods

3.1. Magnetic Susceptibility

[9] Magnetic susceptibility and its anisotropy were first measured on all discrete samples using a KappaBridge KLY-3S susceptometer. Anisotropy of magnetic susceptibility (AMS) is represented by a symmetrical second-rank tensor, which is described by a triaxial ellipsoid with the principal eigenvectors, $k_{max} > k_{int} > k_{min}$, corresponding to the maximum, intermediate, and minimum susceptibility axes, respectively. The mean susceptibility (k) is defined as the mean of k_{max}, k_{int}, and k_{min}. Degree of anisotropy P_j and the shape parameter q were calculated from the magnitude of the three eigenvectors; see *Tarling and Hrouda* [1993, Table 1.1] for the definition of these parameters. A foliated ellipsoid with $q < 0.67$ and k_{min} direction lying within 25° of the vertical are empirically considered to be indicative of primary sedimentary fabric [*Tarling and Hrouda*, 1993].

3.2. S and k_{ARM}/SIRM Ratios

[10] ARM with a peak alternating field of 80 mT and a direct-current (DC) bias field of 0.1 mT was imparted and measured using a cryogenic magnetometer system (2G Enterprises model 760R) of the Geological Survey of Japan, AIST. ARM susceptibility (k_{ARM}) was calculated by normalizing ARM intensity with the strength of the DC field. Next, an IRM was imparted to the samples in a 2.5 T inducing field using a pulse magnetizer (2G Enterprises

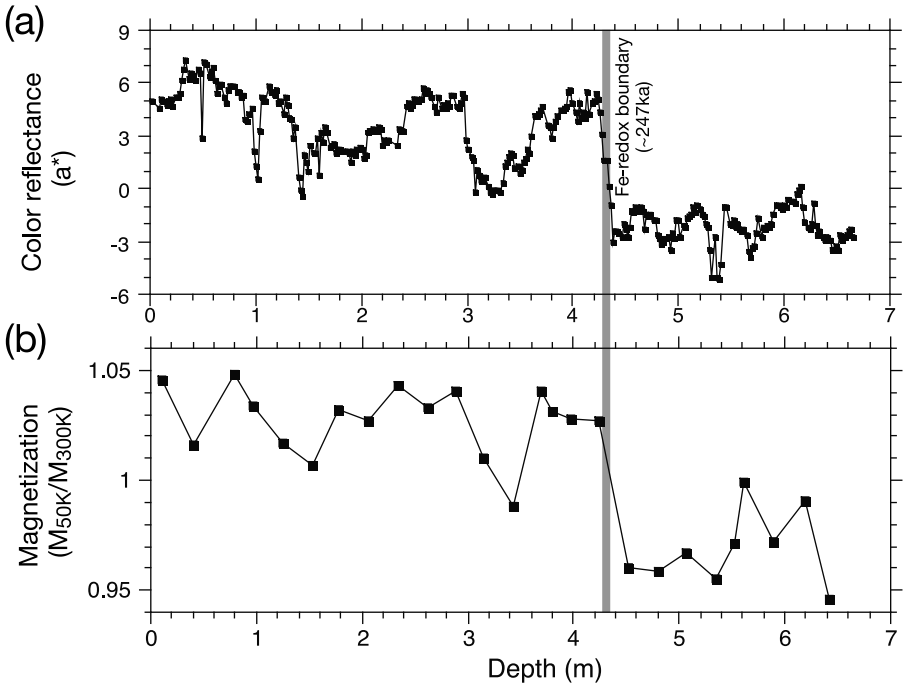

Figure 2. (a) Variations of color reflectance a* with depth in core MR03K04-PC5. Positive (negative) values express reddish (greenish) color. A sharp color change at 4.3 m in depth is indicative of the Fe-redox boundary. (b) The ratio of IRMs at 50 K and 300 K, measured during zero-field cooling of IRM acquired at 300 K. The ratio reflects relative abundance of maghemite to magnetite.

model 660). Here the IRM acquired in a 2.5 T field is regarded as saturation IRM (SIRM). IRMs of 0.1 and 0.3 T were then successively imparted in the direction opposite to the initial IRM. The IRMs were measured using a spinner magnetometer (Natsuhara-Giken SMM-85). HIRM (high-coercivity fraction of IRM) and S ratio ($S_{-0.1T}$) were calculated according to the definition of *Bloemendal et al.* [1992]; HIRM represents abundance of high-coercivity (>0.3 T) magnetic minerals, and $S_{-0.1T}$ is the ratio of low-coercivity to middle- and high-coercivity mineral magnetization. Low-, middle-, and high coercivity minerals are exemplified by magnetite, maghemite, and hematite, respectively. The ratio of k_{ARM} to SIRM (or magnetic susceptibility) has been widely used as a proxy of magnetic grain size since *Banerjee et al.* [1981] and *King et al.* [1982]. On interpreting the k_{ARM} /SIRM ratio, however, it should be taken into consideration that this ratio is also controlled by the strength of magnetostatic interactions among magnetic grains because ARM acquisition is sensitive to the strength of magnetostatic interactions [*Sugiura*, 1979; *Yamazaki and Ioka*, 1997; *Yamazaki*, 2008].

3.3. FORC Diagram

[11] To characterize magnetic mineral assemblages in the samples, FORC measurements [*Pike et al.*, 1999; *Roberts et al.*, 2000] were conducted using an alternating gradient magnetometer (AGM, Princeton Measurements Corporation MicroMag 2900). The measurements were conducted on dried specimens taken at about 10 cm intervals, with a total of 70 specimens. A field spacing between measurements was set to 0.5 mT, and a total of 191 FORCs were measured, with coercivity (H_c) between 0 and 60 mT, and local interaction field (H_u) between −15 and 15 mT. The narrow field spacing was adopted to precisely depict the shape of the peak near the H_c axis that represents a non-interacting SD grain assemblage [*Egli et al.*, 2010]. The maximum applied field was 1.0 T. The averaging time spent at each data point was 200 ms. A smoothing factor (SF) [*Roberts et al.*, 2000] of 3 was used. The FORCIT software of *Acton et al.* [2007] was used for data processing.

[12] For semiquantitative estimation of the relative contribution of the interacting (I) and non-interacting (N-I) components from the FORC diagrams, the same procedure as that of *Yamazaki* [2008, 2009, 2012] was adopted: curve fitting of a cross-section that parallels the H_u axis and that crosses the peak of H_c. It was assumed that the profile consists of three components, the SD N-I and I components, and a multidomain (MD) component, each with a Gaussian distribution of H_u. The standard deviation of each component was fixed to be 0.7 mT (N-I component), 6 mT (I component), and 23 mT (MD component), respectively, following *Yamazaki* [2008], and the relative abundance of the three components was varied by trial and error so as to achieve an optimal fit, which is similar to the fitting method in the IRM decomposition process of *Kruiver et al.* [2001]. Here we assumed that the I component, which is represented by the vertical spread at the foot of the central ridge, is carried by an assemblage of interacting SD grains, but it may also be carried by pseudo-single-domain (PSD) grains. The MD component is represented nearly as a constant on these cross-sections. The lower half (negative H_u) of the FORC diagrams was used for the component fitting.

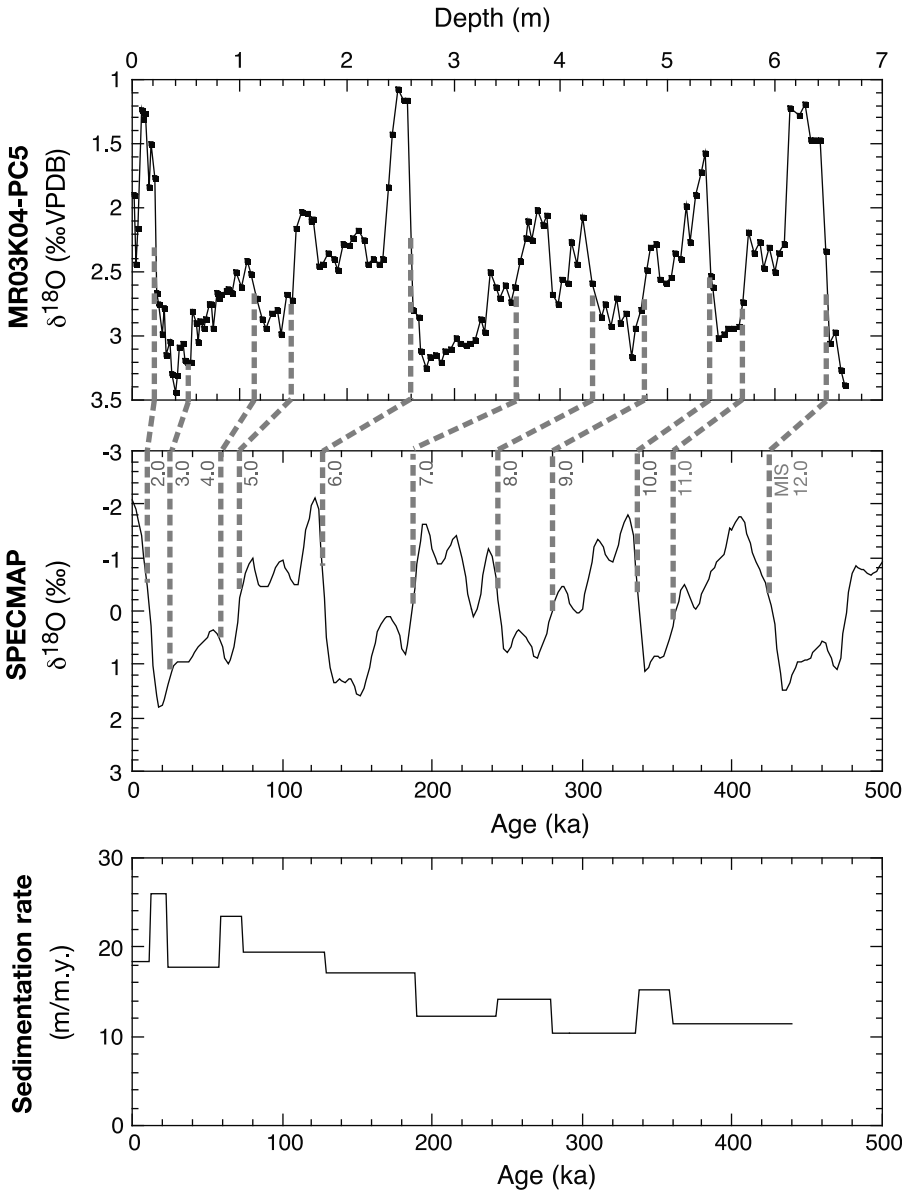

Figure 3. (top) Oxygen-isotope ratio (δ^{18}O) of core MR03K04-PC5 in a depth scale, (middle) correlation to the SPECMAP stack [*Imbrie et al.*, 1984] and (bottom) temporal variations of sedimentation rates based on the correlation. The sedimentation rate between the tie points was assumed to be uniform.

3.4. IRM Acquisition

[13] IRM acquisition curves were measured using the AGM to estimate magnetic mineral composition. The experiments were conducted on the same specimens used for the FORC measurements. One hundred measurements were made at equidistant field steps on a log-scale ranging from 3 mT to 1.4 T. The IRM acquisition curves were decomposed into magnetic coercivity components using the method of *Kruiver et al.* [2001] assuming that the IRM acquisition curves are a linear addition of components represented by cumulative log-Gaussian functions. This method is a kind of forward modeling, and hence there is arbitrariness for the choice of the number of components and a mean coercivity and dispersion parameter (DP) of individual components. For pelagic sediments in the Pacific Ocean, the IRM acquisition curves could be described in general by two dominant components, a low-coercivity (L1) component with a mean coercivity of ~40 mT and DP of ~0.2 and a middle-coercivity (M) component with a mean coercivity of ~100 mT and DP of ~0.3, and two other components, a very-low-coercivity (VL) component with a mean coercivity of ~15 mT and a high-coercivity (H) component with a mean coercivity of >0.4 T [*Yamazaki*, 2008, 2009]. Occasionally another component (L2) with a mean coercivity of ~65 mT and conspicuously narrow DP of ~0.1 was required [*Yamazaki*, 2012]. In this study, we adopted components with mean coercivities and DPs similar to those in the Pacific pelagic sediments, and examined if the observations were satisfied with changing their relative abundance.

3.5. Low-Temperature Measurement

[14] In order to obtain further information on magnetic mineralogy, low-temperature magnetic measurements were made on 26 dried specimens taken at 20 to 40 cm intervals using a low-temperature superconducting quantum interference device (SQUID) susceptometer (Quantum Design MPMS-XL5). An IRM was imparted at 300 K in a 2.5 T field, and magnetization during cycling the temperature between 300 and 6 K in a nearly zero field was measured.

[15] *Özdemir and Dunlop* [2010] proposed that low-temperature measurement is useful for estimating degree of oxidation of magnetite grains. They documented that IRM of maghemite acquired at room temperature monotonically increases with decreasing temperature, whereas that of stoichiometric magnetite decreases from room temperature to the Verwey transition at ~120 K. When a magnetic mineral assemblage is a mixture of maghemite and magnetite, the magnetization curve during low-temperature cycling is a superposition of the two, and hence the shape of the curve reflects the relative abundance of the two minerals.

3.6. TEM Observation

[16] Magnetic minerals extracted from the sediments at 1.88, 2.78, 3.78, and 4.42 m in depth were observed using a transmission electron microscope (TEM) in order to examine abundance and shape of biogenic magnetites preserved in the sediments. Magnetites of biogenic origin were identified based on the characteristic morphologies (octahedron, parallelepiped, and tear-drop shape), sizes within an SD range, that is, several tens of nanometer, and alignment of grains in a chain [*Petersen et al.*, 1986; *Stolz et al.*, 1986]. Morphology of biogenic magnetites can be a sensitive indicator of slight oxic-suboxic environmental fluctuations in sediments; the proportion of biogenic magnetites with parallelepiped and teardrop shapes increases in less oxic conditions compared with those with octahedral morphology [*Hesse*, 1994; *Yamazaki and Kawahata*, 1998; *Egli*, 2004b; *Yamazaki*, 2012].

[17] To carry out magnetic separation, sediments were dispersed completely in water with sodium-hexametaphosphate using an ultrasonic bath. Magnetic fraction was collected by circulating the dispersed sediments through a region of a high magnetic field gradient. The magnetic extracts were dispersed in ethanol, and a small drop of the suspension was dried on a carbon-coated copper grid for TEM observation. The samples were examined on a Topcon EM002B TEM operating at 120 keV.

4. Results

4.1. Magnetic Susceptibility

[18] Magnetic susceptibility of core MR03K04-PC5 increases in glacial periods (Figure 4b). The glacial-interglacial variation pattern of this core agrees well with that of nearby cores in the south Indian Ocean [*Kent*, 1982; *Dezileau et al.*, 2000; *Mazaud et al.*, 2010]. This indicates that magnetic susceptibility variations of this core represent regional, but not local, fluctuations of magnetic mineral concentration. Dilution effect by non-magnetic minerals on the magnetic susceptibility variations is minor in this region [Mazaud et al., 2010]. Furthermore, the magnetic susceptibility variation pattern closely resembles that of the Subtropical South Atlantic susceptibility (SUSAS) stack [*Schmieder et al.*, 2000] (Figure 4b), which was constructed using 12 cores taken between 22°S and 34°S in the subtropical South Atlantic. This coincidence indicates that the abundance of magnetic minerals in the studied core is controlled by a mechanism working commonly in the South Atlantic and south Indian Ocean. The magnetic susceptibility variations resemble those of eolian dust flux recorded in Antarctic ice cores (Figure 4a), as pointed out previously [*Petit et al.*, 1990; *Bareille et al.*, 1994; *Pugh et al.*, 2009; *Weber et al.*, 2012].

[19] Degree of AMS is small in general, less than 1.02 (Figure 4g). It shows a tendency to increase in interglacial periods, in particular during MISs 9 and 11. The samples with the shape parameter q of larger than 0.67 or k_{min} inclination smaller than 65° were excluded because they were judged as sedimentary fabric not having been preserved. The lacking data between ca. 220 and 260 ka correspond to the interval of deformed core-liner.

4.2. FORC Diagram and k_{ARM}/SIRM Ratio

[20] FORC diagrams of all specimens have a narrow ridge along the H_c axis with very small vertical spread (Figure 5). This indicates very weak magnetostatic interaction [*Roberts et al.*, 2000], and is the characteristic of biogenic magnetite [*Egli et al.*, 2010; *Roberts et al.*, 2011]. Biogenic magnetites preserved in sediments as isolated chains are magnetically equivalent to non-interacting SD particles because all magnetite crystals in individual chains simultaneously switch at a critical field. The mean of H_c values at the peak of the FORC distributions is approximately 29 mT, which is typical of the coercivity of SD magnetite.

[21] When plotting the I/N-I component ratio versus the k_{ARM}/SIRM ratio, the two are inversely correlated (Figure 6); specimens with high k_{ARM}/SIRM ratio tend to have a smaller proportion of the I component, although it is difficult to recognize slight differences in the vertical spread at the foot of the ridge that represents the I component among the three FORC diagrams in Figure 5. Data from core MR03K04-PC5 are distributed on the trend common to pelagic sediments in the Pacific including the central North Pacific along 175°E longitude, eastern equatorial Pacific at Integrated Ocean Drilling Program (IODP) Site 1337, Ontong-Java Plateau in the western equatorial Pacific, and Manihiki Plateau in the South Pacific [*Yamazaki*, 2009; *Yamazaki and Solheid*, 2011; *Yamazaki*, 2012] (Figure 6). This correlation indicates that the k_{ARM}/SIRM ratio is dominantly controlled by the strength of magnetostatic interactions. According to *Yamazaki* [2008, 2009, 2012], the k_{ARM}/SIRM ratio is interpreted to reflect the relative abundance of the non-interacting biogenic component and interacting terrigenous component in sediments.

[22] Downcore variations of the k_{ARM}/SIRM ratio show decreases in glacial periods, although the glacial-interglacial changes become obscure below the Fe-redox boundary (Figure 4c). This suggests that relative abundance of the terrigenous component increases in glacial periods. Values of the k_{ARM}/SIRM ratio in core MR03K04-PC5 are lower in general than those of the eastern equatorial Pacific and Manihiki Plateau, but higher than those of the Ontong-Java Plateau and North Pacific (Figure 6). The differences of the positions along the inverse trend on the I/N-I component

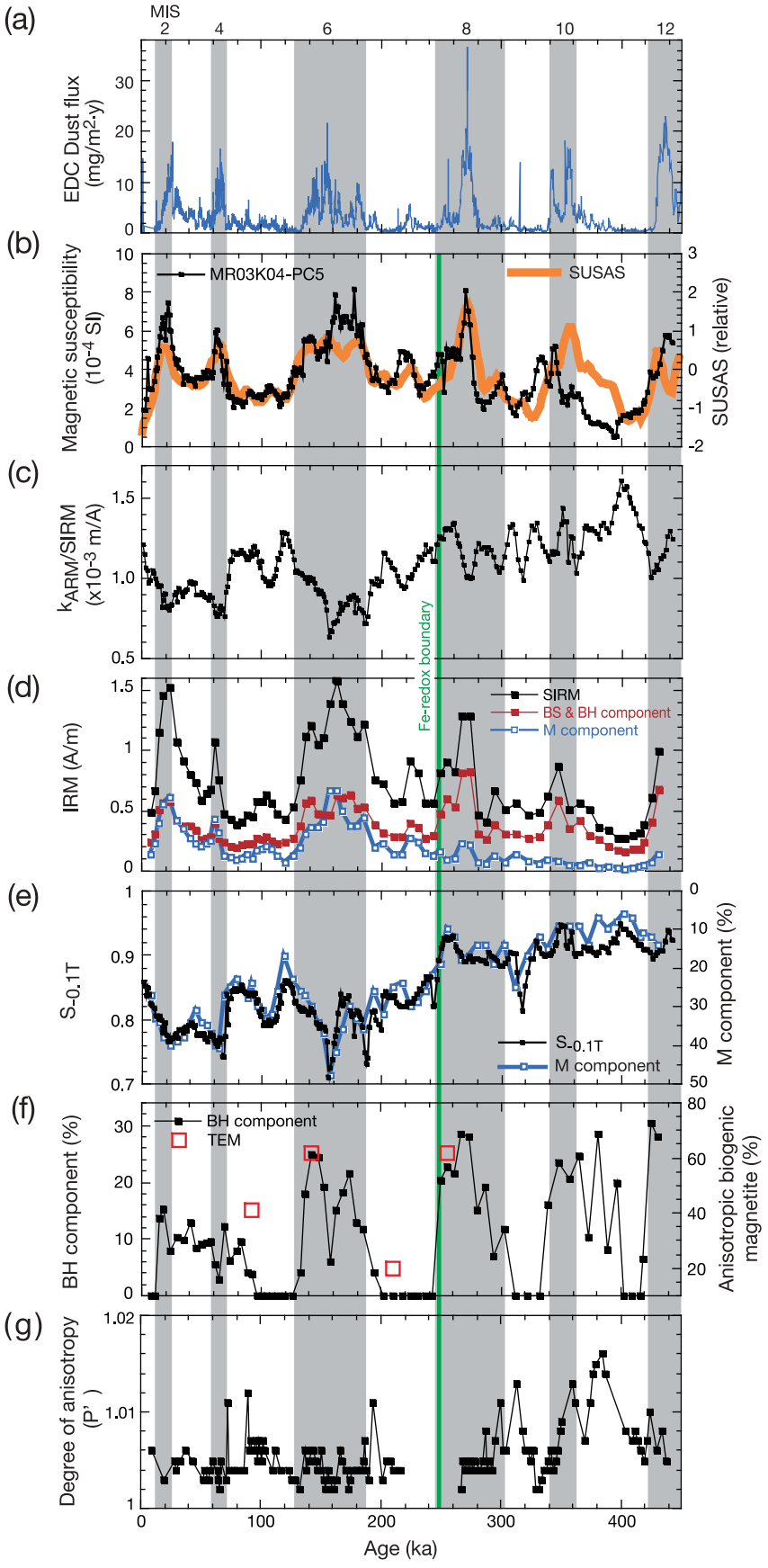
(a)
MIS
2
4
6
8
10
12
EDC Dust flux (mg/m2.y)
(b)
Magnetic susceptibility (10-4 SI)
MR03K04-PC5
SUSAS
SUSAS (relative)
(c)
kARM/SIRM (x10-3 m/A)
Fe-redox boundary
(d)
IRM (A/m)
SIRM
BS & BH component
M component
(e)
S-0.1T
S-0.1T
M component
M component (%)
(f)
BH component (%)
BH component
TEM
Anisotropic biogenic magnetite (%)
(g)
Degree of anisotropy (P')
0
100
200
300
400
Age (ka)

Figure 4

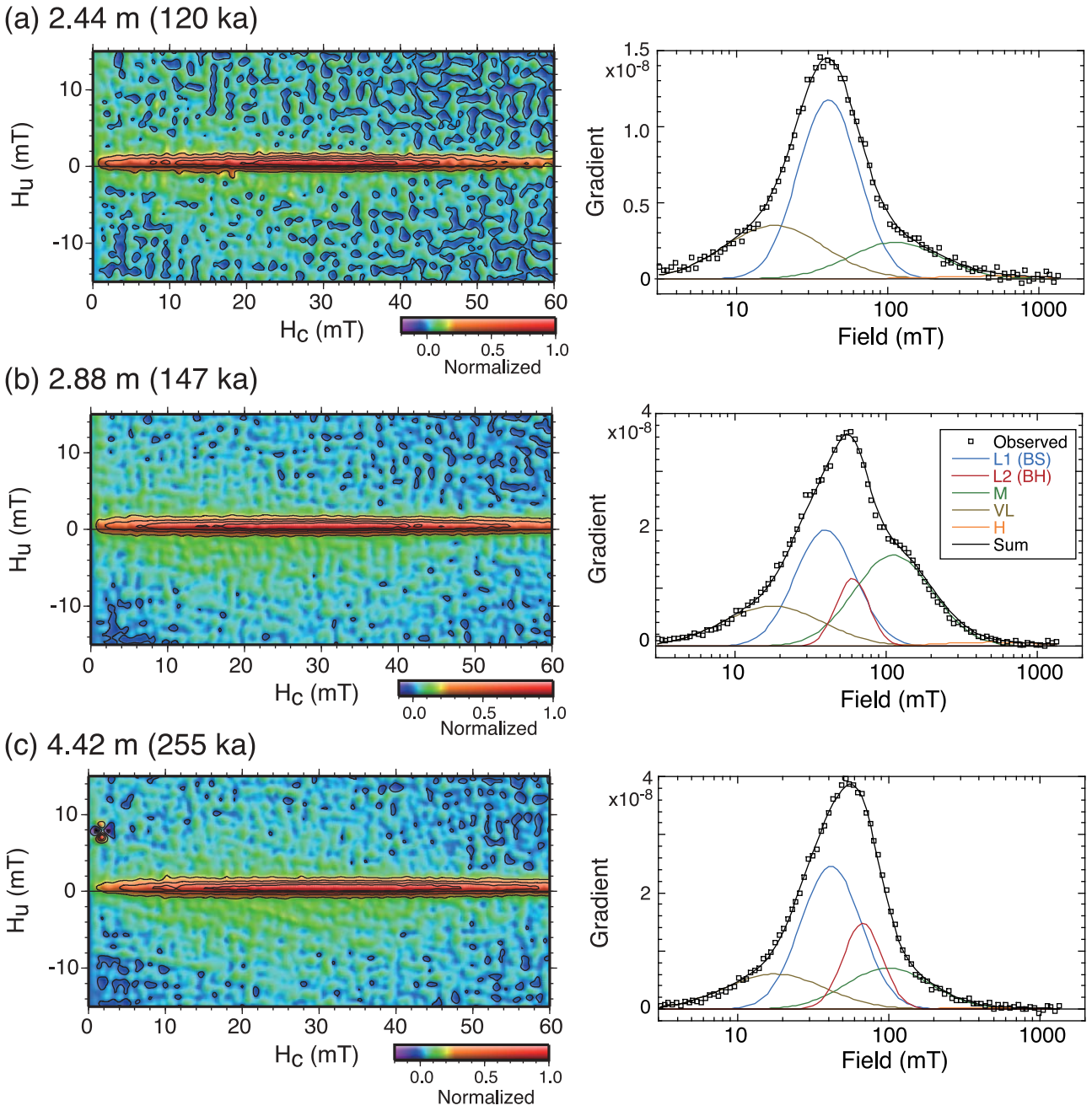

Figure 5. (a–c) Examples of high-resolution FORC diagrams (left) and corresponding IRM component analyses (right). For IRM component analyses, squares represent data points that define the gradient of the IRM acquisition curves, which can be described by the sum (black curve) of two dominant components, low-coercivity (L1, blue curve) and middle-coercivity (M, green) components, two other components, very-low-coercivity (VL, brown) and high-coercivity (H, orange) components, and occasionally another low-coercivity component with conspicuously narrow dispersion (L2, red).

Figure 4. (a) Dust flux of EPICA Dome C ice core [*Lambert et al.*, 2008] and (b–g) temporal variations of magnetic properties. (b) Magnetic susceptibility of core MR03K04-PC5 (black) and the subtropical South Atlantic susceptibility (SUSAS) stack [*Schmieder et al.*, 2000] (orange). (c) The ratio of ARM susceptibility (k_{ARM}) to SIRM. (d) SIRM (black), IRM carried by the biogenic soft (BS) and biogenic hard (BH) components (red), and IRM carried by the middle-coercivity (M) component (blue), derived from IRM component analyses. (e) $S_{-0.1T}$ (black) and the proportion of M component (blue, inverted axis) from IRM component analyses. (f) The proportion of the BH component (black) and the proportion of crystals with anisotropic morphologies among biogenic magnetites on TEM images (red square). (g) Degree of magnetic susceptibility anisotropy. The Fe-redox boundary occurs at ~250 ka. Periods of even Marine Isotope Stage (MIS) numbers are shaded.

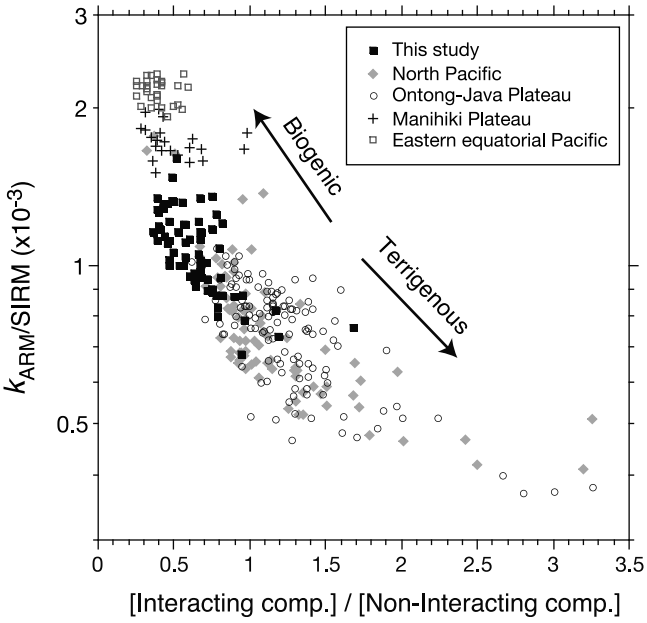

Figure 6. Relationship between the k_{ARM}/SIRM ratio and the proportion of interacting (I) to non-interacting (N-I) SD components derived from FORC diagrams. Solid squares: core MR03K04-PC5, diamonds: data from the central North Pacific [*Yamazaki*, 2008], circles: Ontong-Java Plateau in the western equatorial Pacific [*Yamazaki*, 2009; *Yamazaki and Solheid*, 2011], crosses: Manihiki Plateau in the South Pacific [*Yamazaki*, 2009], squares: IODP Site 1337 in the eastern equatorial Pacific [*Yamazaki*, 2012].

ratio versus the k_{ARM}/SIRM ratio diagram reflect differences in the contribution of the terrigenous component.

4.3. IRM Acquisition and S Ratio

[23] The IRM component analyses revealed that differences in the shape of IRM acquisition curves can be explained by varying relative abundance of the components that appeared in Pacific pelagic sediments [*Yamazaki*, 2008, 2009, 2012] without changing significantly the mean coercivities and DPs (Figure 5). The most dominant is the low-coercivity (L1) component with a mean coercivity of ~40 mT and DP of ~0.2. The second is the middle-coercivity (M) component with a mean coercivity of ~100 mT and DP of 0.27–0.30. Occasionally the gradient of the IRM acquisition curves showed a skewed shape, and in such case another component (L2) with a mean coercivity of 60–70 mT and conspicuously narrow DP of 0.10–0.13 was required (Figures 5b and 5c). In addition, the very-low-coercivity component (VL) with a mean coercivity of ~15 mT, and the high-coercivity component (H) with a mean coercivity of >0.4 T were required for optimal fitting.

[24] We interpret that the L1 and L2 components correspond to the biogenic soft (BS) and biogenic hard (BH) components of *Egli* [2004a], respectively, from the mean coercivities and DPs of the two components and the k_{ARM}/SIRM ratios [*Yamazaki*, 2012]. The BS and BH components probably correspond to different morphologies of magnetosomes; equant octahedron would correspond to the BS component, and elongated morphologies such as parallelepiped and teardrop are expected to have higher coercivities and thus correspond to the BH component. Downcore variations of the proportion of the BH component show increases in glacial periods (Figure 4f). As the spices of magnetotactic bacteria that produce magnetosomes of elongated morphologies would prefer less oxic conditions [*Hesse*, 1994; *Yamazaki and Kawahata*, 1998; *Egli*, 2004b; *Yamazaki*, 2012], the increased BH component in glacials suggests increased ocean productivity, which is consistent with the increased sedimentation rates.

[25] The proportion of the M component varies in parallel with inverted $S_{-0.1T}$ variations (Figure 4e). This is consistent with the observation that the M component has a mean coercivity of ~100 mT. The M component is interpreted to correspond to the I component derived from the FORC diagrams, and be carried by terrigenous maghemites [*Yamazaki*, 2008, 2009, 2012]. This is supported by the positive correlation between the proportion of the M component and the I/N-I component ratio for the samples above the Fe-redox boundary (Figure 7a). Furthermore, IRM carried by the M component shows strong linear correlation with HIRM (Figure 7b). HIRM is indicative of magnetization carried by hematite, which is considered to be of terrigenous origin. This reinforces the interpretation that the M component represents terrigenous input.

[26] The relative abundance of the M component increases in glacial periods above the Fe-redox boundary, and S ratio ($S_{-0.1T}$) decreases in the same periods of time. This implies increases of the proportion of the terrigenous component in glacials. Maghemite-to-magnetite reduction at the Fe-redox boundary is responsible for the sudden downcore increase of $S_{-0.1T}$ and decrease of the M component there.

4.4. Low-Temperature Measurement

[27] For specimens above 4.3 m in depth, magnetization at temperatures below the Verwey transition temperature (T_v) remains larger than the IRM at 300 K during cooling (Figure 8, top), whereas magnetization becomes smaller than the initial IRM for specimens below this depth (Figure 8, bottom). This indicates smaller degree of maghemitization for the latter. To quantify the differences in the shape of the magnetization curves, the ratio of IRMs at 50 K to 300 K (IRM_{50K}/IRM_{300K}) was used here as a proxy for the relative abundance of maghemite and magnetite [*Özdemir and Dunlop*, 2010; *Yamazaki and Solheid*, 2011]. The IRM_{50K}/IRM_{300K} ratio suddenly decreases downcore at about 4.3 m in depth (~247 ka) (Figure 2b). This indicates that the proportion of maghemite to magnetite decreases there, and supports the occurrence of the Fe-redox boundary at this depth inferred from the core color change. The decrease in the proportion of maghemite at this depth is consistent with the coeval decrease of the M component and increase of $S_{-0.1T}$ (Figure 4e). A decrease of the IRM_{50K}/IRM_{300K} ratio can also be caused by a decrease in the concentration of superparamagnetic (SP) grains, but the coincidence with sediment color change and variations in the M component and $S_{-0.1T}$ prefers explanation by maghemite-to-magnetite reduction. A change in color reflectance a* toward the greenish side and a decrease in the IRM_{50K}/IRM_{300K} ratio around 3.3 m, about 1 m above the Fe-redox boundary, may represent a relict of past episodes of nonsteady state oxic-suboxic changes.

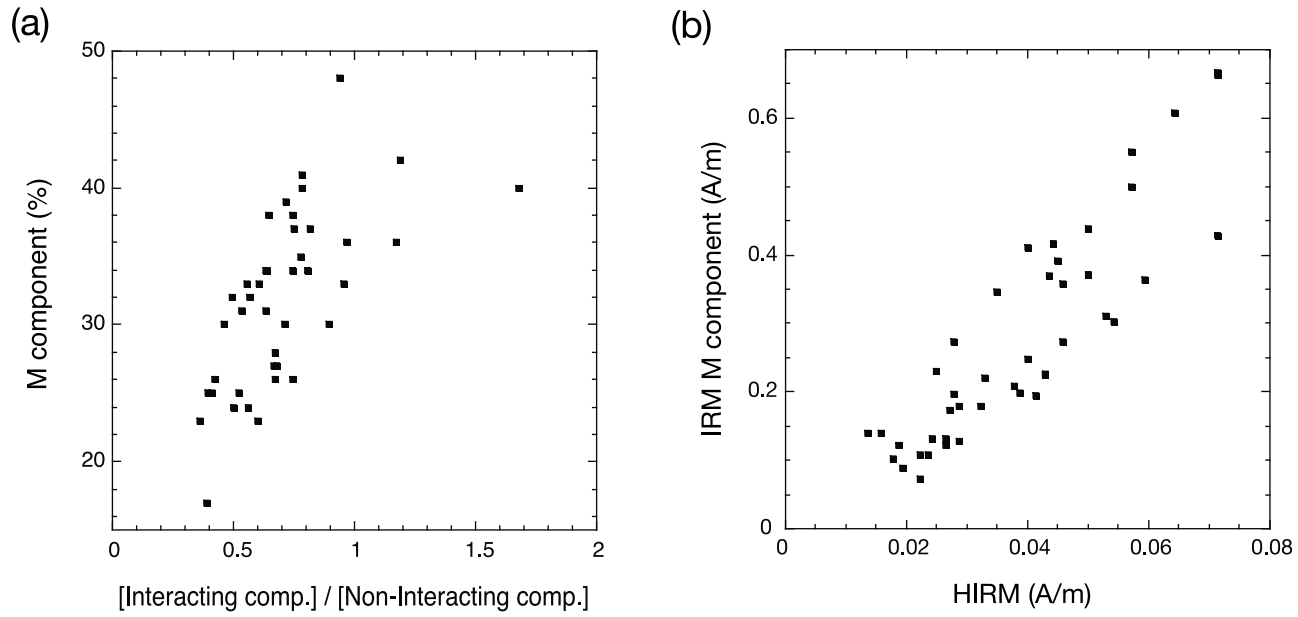

Figure 7. (a) Relationship between the proportion of the interacting SD component (I component) to the non-interacting SD component (N-I component) derived from FORC diagrams and the proportion of the middle-coercivity component (M component) derived from IRM component analyses. (b) Relationship between HIRM (high-coercivity fraction of IRM), which is presumably carried by hematite, and IRM carried by the M component.

4.5. TEM Observation

[28] Under TEM, biogenic magnetites were the major constituent of magnetic minerals in the samples examined; their occurrence is abundant (Figure 9). Biogenic magnetites were identified based on the characteristic morphologies (octahedron, parallelepiped, and teardrop shape) and sizes within an SD range [*Petersen et al.*, 1986; *Stolz et al.*, 1986]. Equant octahedral magnetites can be produced also by abiological processes, but their almost identical sizes confined within an SD range are indicative of bacterial origin.

[29] We grouped the biogenic magnetites into isotropic (equant octahedron) and anisotropic based on their morphologies under TEM images (Figure 9). The latter group was subdivided into parallelepiped and teardrop. In total, 200 to 400 grains were counted for each sample. Although the limited number of TEM images through the magnetic extraction procedure may not represent faithfully the original magnetic mineral assemblages and hence the estimation of relative abundance by the counts is semi-quantitative at most, differences in dominant morphology among the extracts can be recognized even visually on the TEM images (Figure 9). Differences in the proportion of anisotropic biogenic magnetites for the four samples are consistent with the variations of the BH component of the IRM component analyses (Figure 4f). This supports the inference that the BH component is carried by biogenic magnetites with elongated morphologies, and indicates that IRM acquisition curves are very useful for estimating morphological constitution of biogenic magnetite assemblages in sediments, which varies sensitively with oxic-suboxic environmental fluctuations [*Egli*, 2004b; *Yamazaki*, 2012]. The sample just below the Fe-redox boundary did not show evidence for dissolution of biogenic magnetites on the TEM images (Figure 9b).

5. Discussion

[30] Environmental magnetic measurements including FORC diagrams, IRM component analyses, k_{ARM}/SIRM ratios, and TEM observations revealed that magnetization of core MR03K04-PC5 in the south Indian Ocean is carried by the magnetic components similar to those observed commonly in Pacific pelagic sediments. The magnetic mineral assemblage is dominated by biogenic magnetites. Magnetic mineral concentration increased in glacial periods, which is accompanied by increased proportion of the terrigenous component. These magnetic property changes should have global significance, as indicated by the observation that the magnetic susceptibility variations of core MR03K04-PC5 resemble those of other cores in the Southern Ocean and mimics the SUSAS stack constructed in the subtropical South Atlantic and eolian dust flux records from Antarctic ice cores. We here discuss paleoceanographic mechanisms underlying the magnetic property changes. The discussion is limited to the period of time above the Fe-redox boundary, younger than ca 250 ka. Maghemite-to-magnetite reduction at the boundary might affect the k_{ARM}/SIRM ratio, although the case study of Ontong-Java Plateau sediments suggested that the k_{ARM}/SIRM ratio was not influenced significantly [*Yamazaki and Solheid*, 2011].

[31] It is suggested that in the Southern Ocean today's ocean productivity is limited by deficiency of iron, and that increased iron input derived as eolian dust fueled primary productivity in glacial periods [*Martin*, 1990; *Kumar et al.*,

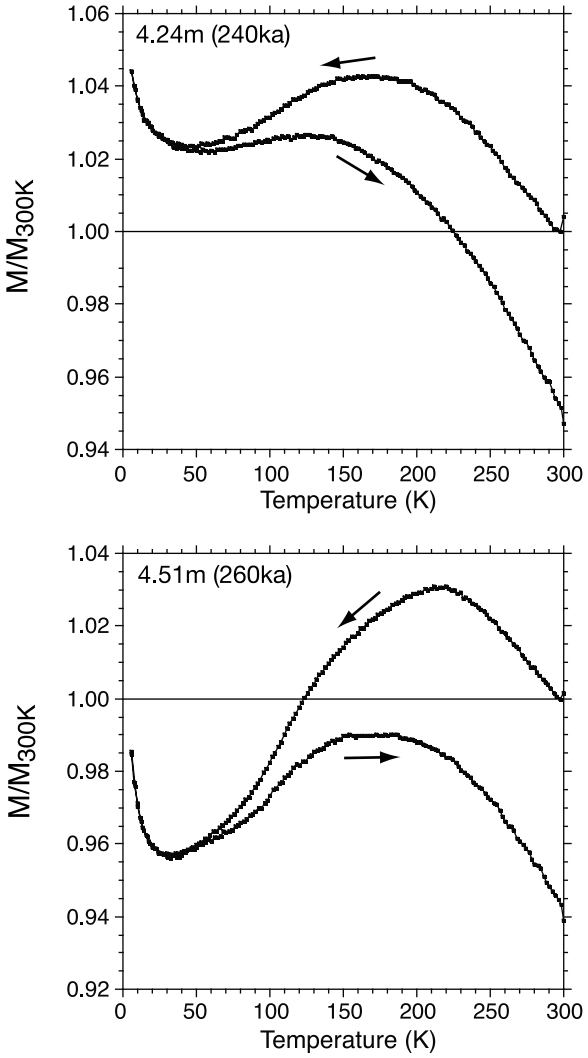

Figure 8. Changes of IRM imparted at 300 K with cycling temperature between 300 and 6 K, normalized by the magnetization intensity at 300 K, just (top) above and (bottom) below the Fe-redox boundary.

1995; *Cassar et al.*, 2007; *Martínez-Garcia et al.*, 2009]. *Roberts et al.* [2011] proposed that the abundance of biogenic magnetites is controlled by the iron fertilization based on a study of Eocene sediments obtained from the Kerguelen Plateau in the south Indian Ocean. They found correlation among the abundance of biogenic magnetites, eolian dust flux, and ocean productivity inferred from the abundance of eutrophic species of calcareous microfossils. They proposed two possible mechanisms for the correlation. First, increased ocean productivity by iron fertilization is likely to have increased export of organic carbon to the seafloor, which would have fueled magnetotactic bacterial metabolism. Second, dissolved iron from sediments in an iron-reducing environment, which was promoted by increased ocean productivity, would have become a source of iron necessary for magnetosome biomineralization.

[32] We consider that the increased magnetic concentration in glacial periods in the Southern Ocean can be explained by this mechanism: increased biogenic magnetite production associated with increased eolian dust. In core MR03K04-PC5, biogenic magnetites are the most dominant magnetic constituent, and the variations of magnetic mineral concentration represented by IRM are mainly controlled by the amount of the biogenic component. The abundance of both biogenic and terrigenous magnetic minerals increased in glacial periods (Figure 4d), although relative contribution of the biogenic component decreased because the increase of the terrigenous component surpassed that of the biogenic component. Ocean productivity is known to have increased in glacials in the subantarctic zone of the Southern Ocean [*Anderson et al.*, 2002]. The glacial increases of the BH component representing elongated magnetofossil morphology and the sedimentation rates in core MR03K04-PC5 suggest that glacial increases in ocean productivity occurred also at this site.

[33] The resemblance between the magnetic concentration variations in the circum-Antarctic ocean and the SUSAS stack in the subtropical Atlantic suggests that these variations are modulated by a common climatic driver. For the SUSAS stack, the magnetic susceptibility variations were explained by dilution effect of calcium carbonate [*Schmieder et al.*, 2000]. In the Atlantic and Southern Ocean sector, carbonate preservation is known to have declined

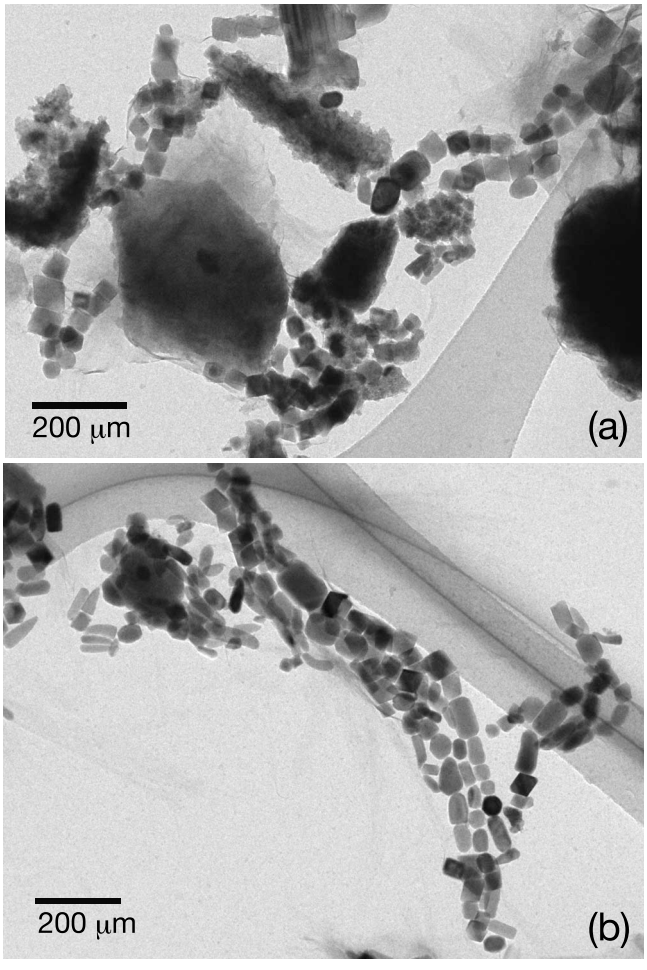

Figure 9. TEM images of magnetic extracts from core MR03K04-PC5 (a) at 3.78 m (203 ka) dominated by equant biogenic magnetites and (b) at 4.42 m (254 ka) dominated by biogenic magnetites with elongated morphologies.

during glacial periods, which is attributed to the spread of the corrosive Circumpolar Deep Water led by decreased influx of the less corrosive NADW [*Volat et al.*, 1980; *Kent*, 1982; *Howard and Prell*, 1994; *Diekmann*, 2007]. The observation of this study that magnetic mineral constituents were also varied with magnetic concentration indicates that the simple dilution model is insufficient. Resemblance of the pattern of the SUSAS stack with dust records from Antarctic ice cores suggests that iron fertilization may have occurred also in the subtropical Atlantic and production of biogenic magnetites was increased, or that biogenic magnetites produced in circum-Antarctic Ocean sediments under iron fertilization were supplied to the subtropical Atlantic through redistribution by bottom water currents.

[34] In the south Indian Ocean east of the Kerguelen and Crozet Plateaus, it is estimated from mineralogical and geochemical data that volcanic detrital materials from the Kerguelen-Crozet province is a major source of terrigenous flux in sediments, which is transported eastward by the ACC [*Bareille et al.*, 1994; *Dezileau et al.*, 2000]. During low sea level stands in glacial periods, the shallow plateau region could have suffered increased erosion and hence caused an increased detrital supply. There is a possibility that in glacial periods increased amount of detrital materials was transported by intensified ACC, which may also have caused higher detrital flux for sediments in the south Indian Ocean [*Dezileau et al.*, 2000]. However, the magnetic mineral assemblage of our core is dominated by biogenic magnetites, and the contribution of volcanic detrital materials is estimated to be small. The hypothesis of dust induced biogenic magnetite production can explain better the close resemblance of the pattern of magnetic concentration variations throughout the Southern Ocean and even in the subtropical Atlantic. Ice-rafted debris (IRD) is also considered not to be a major source of the magnetic susceptibility signals in the Southern Ocean [*Bareille et al.*, 1994; *Diekmann et al.*, 2000]. Core MR03K04-PC5 has no evidence for IRD input; the site at ~41.5°S is far north for a significant amount of icebergs of Antarctic origin to reach. Furthermore, the similarity of magnetic susceptibility signals to the SUSAS stack of 22°S to 34°S in the South Atlantic cannot be explained by variations of IRD input.

[35] *Mazaud et al.* [2010] suggested that ACC intensity controlled the abundance and grain size of magnetic minerals in the south Indian Ocean. They interpreted the variations of the k_{ARM}/SIRM ratio observed in their core as fluctuations of magnetic grain size, and that smaller k_{ARM}/SIRM ratio (representing larger grain size in their interpretation) in glacial periods implies stronger ACC. However, the k_{ARM}/SIRM ratio variations do not necessarily indicate magnetic grain size changes. Alternatively, the k_{ARM}/SIRM ratio reflects difference in the strength of magnetostatic interaction among magnetic grains [*Sugiura*, 1979; *Yamazaki and Ioka*, 1997; *Yamazaki*, 2008]. Our study showed that the composition of magnetic minerals changes associated with glacial-interglacial variations of magnetic mineral concentration, and the variations of the k_{ARM}/SIRM ratio can be explained better by changes in relative abundance of the biogenic and terrigenous components. Degree of AMS in our core showed no evidence for increased bottom water current speed in glacial periods in the south Indian Ocean (Figure 4g); it rather decreased in glacials, which is the opposite to that expected from intensified bottom current [e.g., *Kissel et al.*, 1997].

6. Conclusions

[36] An environmental magnetic study of core MR03K04-PC5 taken from the south Indian Ocean has led the following conclusions.

[37] 1. The pattern of magnetic mineral concentration variations of the core resembles that of other cores in the Southern Ocean, and mimics the SUSAS stack in the subtropical South Atlantic and eolian dust flux records from Antarctic ice cores. The resemblance suggests that these variations are controlled by a common climatic driver.

[38] 2. The k_{ARM}/SIRM ratio represents relative abundance of the interacting and non-interacting magnetic components. The IRM acquisition curves can be explained by the addition of the components with mean coercivities and dispersions similar to those appeared in Pacific pelagic sediments. It is interpreted that the non-interacting and interacting components are carried by low-coercivity magnetites of biogenic origin and middle-coercivity maghemites of terrigenous origin, respectively.

[39] 3. Biogenic magnetites are the most dominant constituent of the magnetic mineral assemblages. In glacial periods, the abundance of both biogenic and terrigenous components increased, whereas the proportion of the biogenic to terrigenous components decreased because the increases of the terrigenous component surpassed those of the biogenic component. Increased ocean productivity in glacial periods is suggested from increased proportions of biogenic magnetites with elongated morphologies, indicative of less oxic conditions, and increased sedimentation rates.

[40] 4. The increased magnetic mineral concentration in glacial periods in the Southern Ocean may be explained by iron fertilization; the production of biogenic magnetites was enhanced associated with increased ocean productivity, which was fueled by increased eolian dust flux.

[41] **Acknowledgments.** We thank Emi Kariya and Etsuko Usuda for help with the magnetic measurements, Noriko Yoshizawa and Akira Takatsuki for conducting TEM observation under "R&D Support Project of Transmission Electron Microscopy" of AIST, and Naomi Harada for providing extra samples for the TEM observation. We also thank Michiyo Kobayashi for stable isotope measurements in Kochi University, and two reviewers, Fabio Florind and Ramon Egli, for constructive comments. The coring and onboard measurements were carried out with cooperation of Naomi Harada, Katsunori Kimoto, and onboard scientists, marine technicians, and crew of R/V *Mirai* MR03-K04 Leg 6. This study was partly supported by the Grant-in-Aid for Scientific Research ((B) 19340156, (C) 14540458) of the Japan Society for the Promotion of Science.

References

Acton, G., A. Roth, and K. L. Verosub (2007), Analyzing micromagnetic properties with FORCIT software, *Eos Trans. AGU*, *88*, 230, doi:10.1029/2007EO210004.

Anderson, R. F., Z. Chase, M. Q. Fleisher, and J. Sachs (2002), The Southern Ocean's biological pump during the Last Glacial Maximum, *Deep Sea Res., Part II*, *49*, 1909–1938, doi:10.1016/S0967-0645(02)00018-8.

Banerjee, S. K., J. King, and J. Marvin (1981), A rapid method for magnetic granulometry with applications to environmental studies, *Geophys. Res. Lett.*, *8*, 333–336, doi:10.1029/GL008i004p00333.

Bareille, G., F. E. Grousset, M. Labracherie, L. D. Labeyrie, and J.-R. Petit (1994), Origin of detrital fluxes in the southeast Indian Ocean during the

last climatic cycles, *Paleoceanography*, *9*, 799–819, doi:10.1029/94PA01946.

Bloemendal, J., J. W. King, F. R. Hall, and S.-J. Doh (1992), Rock magnetism of Late Neogene and Pleistocene deep-sea sediments: Relationship to sediment source, diagenetic processes, and sediment lithology, *J. Geophys. Res.*, *97*, 4361–4375, doi:10.1029/91JB03068.

Carter, L., I. N. McCave, and M. J. M. Williams (2008), Circulation and water masses of the Southern Ocean: A review, in *Antarctic Climate Evolution*, *Dev. Earth Environ. Sci*, vol. 8, edited by F. Florindo and M. Siegert, pp. 85–114, Elsevier, New York, doi:10.1016/S1571-9197(08)00004-9.

Cassar, N., M. L. Bender, B. A. Barnett, S. Fan, W. J. Moxim, H. Levy II, and B. Tilbrook (2007), The Southern Ocean biological response to Aeolian iron deposition, *Science*, *317*, 1067–1070, doi:10.1126/science.1144602.

Dezileau, L., G. Bareille, J. L. Reyss, and F. Lemoine (2000), Evidence for strong sediment redistribution by bottom currents along the southeast Indian ridge, *Deep Sea Res., Part I*, *47*, 1899–1936, doi:10.1016/S0967-0637(00)00008-X.

Diekmann, B. (2007), Sedimentary patterns in the late Quaternary Southern Ocean, *Deep Sea Res., Part II*, *54*, 2350–2366, doi:10.1016/j.dsr2.2007.07.025.

Diekmann, B., G. Kuhn, V. Rachold, A. Abelmann, U. Brathauer, D. K. Fütterer, R. Gersonde, and H. Grobe (2000), Terrigenous sediment supply in the Scotia Sea (Southern Ocean): Response to Late Quaternary ice dynamics in Patagonia and on the Antarctic Peninsula, *Palaeogeogr. Palaeoclimatol. Palaeoecol.*, *162*, 357–387, doi:10.1016/S0031-0182(00)00138-3.

Egli, R. (2004a), Characterization of individual rock magnetic components by analysis of remanence curves. 2. Fundamental properties of coercivity distributions, *Phys. Chem. Earth*, *29*, 851–867.

Egli, R. (2004b), Characterization of individual rock magnetic components by analysis of remanence curves. 3. Bacterial magnetite and natural processes in lakes, *Phys. Chem. Earth*, *29*, 869–884.

Egli, R., A. P. Chen, M. Winklhofer, K. Kodama, and C.-S. Horng (2010), Detection of non-interacting single domain particles using first-order reversal curve diagrams, *Geochem. Geophys. Geosyst.*, *11*, Q01Z11, doi:10.1029/2009GC002916.

Evans, M. E., and F. Heller (2003), *Environmental Magnetism: Principles and Applications of Environmagnetics*, 299 pp., Academic, San Diego, Calif.

Hesse, P. P. (1994), Evidence for bacterial palaeoecological origin of mineral magnetic cycles in oxic and sub-oxic Tasman Sea sediments, *Mar. Geol.*, *117*, 1–17, doi:10.1016/0025-3227(94)90003-5.

Howard, W. R., and W. L. Prell (1994), Late Quaternary $CaCO_3$ production and preservation in the Southern Ocean: Implications for oceanic and atmospheric carbon cycling, *Paleoceanography*, *9*, 453–482, doi:10.1029/93PA03524.

Imbrie, J., J. D. Hays, D. G. Martinson, A. McIntyre, A. C. Mix, J. J. Morley, N. G. Pisias, W. L. Prell, and N. J. Shackleton (1984), The orbital theory of Pleistocene climate: Support from a revised chronology of the marine $\delta^{18}O$ record, in *Milankovitch and Climate, Part I*, edited by A. L. Berger et al., pp. 269–305, D. Reidel, Dordrecht, Netherlands.

Kent, D. V. (1982), Apparent correlation of palaeomagnetic intensity and climatic records in deep-sea sediments, *Nature*, *299*, 538–539, doi:10.1038/299538a0.

King, J., S. K. Banerjee, J. Marvin, and Ö. Özdemir (1982), A comparison of different magnetic methods for determining the relative grain size of magnetite in natural materials: Some results from lake sediments, *Earth Planet. Sci. Lett.*, *59*, 404–419, doi:10.1016/0012-821X(82)90142-X.

Kissel, C., C. Laj, B. Lehman, L. Labyrie, and V. Bout-Roumazeilles (1997), Changes in the strength of the Iceland–Scotland Overflow Water in the last 200,000 years: Evidence from magnetic anisotropy analysis of core SU90–33, *Earth Planet. Sci. Lett.*, *152*, 25–36, doi:10.1016/S0012-821X(97)00146-5.

Kruiver, P. P., M. J. Dekkers, and D. Heslop (2001), Quantification of magnetic coercivity components by the analysis of acquisition curves of isothermal remanent magnetization, *Earth Planet. Sci. Lett.*, *189*, 269–276, doi:10.1016/S0012-821X(01)00367-3.

Kumar, M., R. F. Anderson, R. A. Mortlock, P. N. Froelich, P. Kubik, D. Dittrich-Hannen, and M. Suter (1995), Increased biological productivity and export production in the glacial Southern Ocean, *Nature*, *378*, 675–680, doi:10.1038/378675a0.

Lambert, F., B. Delmonte, J. R. Petit, M. Bigler, P. R. Kaufmann, M. A. Hutterli, T. F. Stocker, U. Ruth, J. P. Steffensen, and V. Maggi (2008), Dust-climate couplings over the past 800,000 years from the EPICA Dome C ice core, *Nature*, *452*, 616–619, doi:10.1038/nature06763.

Martin, J. H. (1990), Glacial-interglacial CO_2 change: The iron hypothesis, *Paleoceanography*, *5*, 1–13, doi:10.1029/PA005i001p00001.

Martínez-Garcia, A., A. Rosell-Melé, W. Geibert, R. Gersonde, P. Masqué, V. Gaspari, and C. Barbante (2009), Links between iron supply, marine productivity, sea surface temperature, and CO_2 over the last 1.1 Ma, *Paleoceanography*, *24*, PA1207, doi:10.1029/2008PA001657.

Mazaud, A., C. Kissel, C. Laj, M. A. Sicre, E. Michel, and J. L. Turon (2007), Variations of the ACC-CDW during MIS3 traced by magnetic grain deposition in midlatitude South Indian Ocean cores: Compositions with the northern hemisphere and with central America, *Geochem. Geophys. Geosyst.*, *8*, Q05012, doi:10.1029/2006GC001532.

Mazaud, A., E. Michel, F. Dewilde, and J. L. Turon (2010), Variations of the Antarctic Circumpolar Current intensity during the past 500 ka, *Geochem. Geophys. Geosyst.*, *11*, Q08007, doi:10.1029/2010GC003033.

Orsi, A. H., T. Whitworth III, and W. D. Nowlin Jr. (1995), On the meridional extent and fronts of the Antractic Circumpolar Current, *Deep Sea Res., Part I*, *42*, 641–673, doi:10.1016/0967-0637(95)00021-W.

Özdemir, Ö., and D. J. Dunlop (2010), Hallmarks of maghemitization in low-temperature remanence cycling of partially oxidized magnetite nanoparticles, *J. Geophys. Res.*, *115*, B02101, doi:10.1029/2009JB006756.

Petersen, N., T. von Dobeneck, and H. Vali (1986), Fossil bacterial magnetite in deep-sea sediments from the South Atlantic Ocean, *Nature*, *320*, 611–615, doi:10.1038/320611a0.

Petit, J. R., L. Mounier, J. Jouzel, Y. S. Korotkevich, V. I. Kotlyakov, and C. Lorius (1990), Palaeoclimatological and chronological implications of the Vostok core dust record, *Nature*, *343*, 56–58, doi:10.1038/343056a0.

Pike, C. R., A. P. Roberts, and K. L. Verosub (1999), Characterizing interactions in fine magnetic particle systems using first order reversal curves, *J. Appl. Phys.*, *85*, 6660–6667, doi:10.1063/1.370176.

Pugh, R. S., I. N. McCave, C.-D. Hillenbrand, and G. Kuhn (2009), Circum-Antarctic age modelling of Quaternary marine cores under the Antarctic Circumpolar Current: Ice-core dust-magnetic correlation, *Earth Planet. Sci. Lett.*, *284*, 113–123, doi:10.1016/j.epsl.2009.04.016.

Roberts, A. P., C. R. Pike, and K. L. Verosub (2000), First-order reversal curve diagrams: A new tool for characterizing the magnetic properties of natural samples, *J. Geophys. Res.*, *105*, 28,461–28,475, doi:10.1029/2000JB900326.

Roberts, A. P., F. Florindo, G. Villa, L. Chang, L. Jovane, S. M. Bohaty, J. C. Larrasoaña, D. Heslop, and J. D. Fitz Gerald (2011), Magnetotactic bacterial abundance in pelagic marine environments is limited by organic carbon flux and availability of dissolved iron, *Earth Planet. Sci. Lett.*, *310*, 441–452, doi:10.1016/j.epsl.2011.08.011.

Robinson, S. G. (1986), The late Pleistocene palaeoclimatic record of North Atlantic deep-sea sediments revealed by mineral-magnetic measurements, *Phys. Earth Planet. Inter.*, *42*, 22–47, doi:10.1016/S0031-9201(86)80006-1.

Schmieder, F., T. von Dobeneck, and U. Bleil (2000), The Mid-Pleistocene climate transition as documented in the deep South Atlantic Ocean: Initiation, interim state and terminal event, *Earth Planet. Sci. Lett.*, *179*, 539–549, doi:10.1016/S0012-821X(00)00143-6.

Skinner, L. C., and I. N. McCave (2003), Analysis and modelling of gravity- and piston coring based on soil mechanics, *Mar. Geol.*, *199*, 181–204, doi:10.1016/S0025-3227(03)00127-0.

Stolz, J. F., S.-B. R. Chang, and J. L. Kirschvink (1986), Magnetotactic bacteria and single-domain magnetite in hemipelagic sediments, *Nature*, *321*, 849–851, doi:10.1038/321849a0.

Suganuma, Y., T. Yamazaki, and T. Kanamatsu (2009), South Asian monsoon variability during the past 800 kyr revealed by rock magnetic proxies, *Quat. Sci. Rev.*, *28*, 926–938, doi:10.1016/j.quascirev.2008.12.014.

Sugiura, N. (1979), ARM, TRM and magnetic interactions: Concentration dependence, *Earth Planet. Sci. Lett.*, *42*, 451–455, doi:10.1016/0012-821X(79)90054-2.

Széréméta, N., F. Bassinot, Y. Balut, L. Labeyrie, and M. Pagel (2004), Oversampling of sedimentary series collected by giant piston corer: Evidence and correlations based on 3.5-kHz chirp profiles, *Paleoceanography*, *19*, PA1005, doi:10.1029/2002PA000795.

Tarling, D. H., and F. Hrouda (1993), *The Magnetic Anisotropy of Rocks*, 217 pp., Chapman and Hall, London.

Venuti, A., F. Florindo, A. Caburlotto, E. Strada, F. Talarico, C.-D. Hillenbrand, and M. Hounslow (2011), Late Quaternary sediments from deep-sea sediment drifts on the Antarctic Peninsula Pacific margin: Climatic control on provenance of minerals, *J. Geophys. Res.*, *116*, B06104, doi:10.1029/2010JB007952.

Verosub, K. L., and A. P. Roberts (1995), Environmental magnetism: Past, present, and future, *J. Geophys. Res.*, *100*, 2175–2192, doi:10.1029/94JB02713.

Volat, J.-L., L. Pastouret, and C. Vergnaud-Grazzini (1980), Dissolution and carbonate fluctuations in Pleistocene deep-sea cores: A review, *Mar. Geol.*, *34*, 1–28, doi:10.1016/0025-3227(80)90138-3.

Watkins, S. J., B. A. Maher, and G. R. Bigg (2007), Ocean circulation at the Last Glacial Maximum: A combined modeling and magnetic proxy-based study, *Paleoceanography*, *22*, PA2204, doi:10.1029/2006PA001281.

Weber, M. E., G. Kuhm, D. Sprenk, C. Rolf, C. Ohlwein, and W. Ricken (2012), Dust transport from Patagonia to Antarctica - A new stratigraphic approach from the Scotia Sea and its implications for the last glacial cycle, *Quat. Sci. Rev.*, *36*, 177–188.

Yamazaki, T. (2008), Magnetostatic interactions in deep-sea sediments inferred from first-order reversal curve diagrams: Implications for relative paleointensity normalization, *Geochem. Geophys. Geosyst.*, *9*, Q02005, doi:10.1029/2007GC001797.

Yamazaki, T. (2009), Environmental magnetism of Pleistocene sediments in the North Pacific and Ontong-Java Plateau: Temporal variations of detrital and biogenic components, *Geochem. Geophys. Geosyst.*, *10*, Q07Z04, doi:10.1029/2009GC002413.

Yamazaki, T. (2012), Paleoposition of Intertropical Convergence Zone in the eastern Pacific inferred from glacial-interglacial changes in terrigenous and biogenic magnetic mineral fractions, *Geology*, *40*, 151–154.

Yamazaki, T., and N. Ioka (1997), Environmental rock-magnetism of pelagic clay: Implications for Asian eolian input to the North Pacific since the Pliocene, *Paleoceanography*, *12*, 111–124, doi:10.1029/96PA02757.

Yamazaki, T., and T. Kanamatsu (2007), A relative paleointensity record of the geomagnetic field since 1.6 Ma from the North Pacific, *Earth Planets Space*, *59*, 785–794.

Yamazaki, T., and H. Kawahata (1998), Organic carbon flux controls the morphology of magnetofossils in marine sediments, *Geology*, *26*, 1064–1066, doi:10.1130/0091-7613(1998)026<1064:OCFCTM>2.3.CO;2.

Yamazaki, T., and P. Solheid (2011), Maghemite-to-magnetite reduction across the Fe-redox boundary in a sediment core from the Ontong-Java Plateau: Influence on relative palaeointensity estimation and environmental magnetic application, *Geophys. J. Int.*, *185*, 1243–1254, doi:10.1111/j.1365-246X.2011.05021.x.

M. Ikehara, Center for Advanced Marine Core Research, Kochi University, B200 Monobe, Nankoku, Kochi 783-8502, Japan.

T. Yamazaki, Geological Survey of Japan, National Institute of Advanced Industrial Science and Technology, 1-1-1 Higashi, Tsukuba 305-8567, Japan. (toshi-yamazaki@aist.go.jp)